Electrically Detected Magnetic Resonance Study of Barium and Nitric Oxide Treatments of 4H-SiC Metal-Oxide-Semiconductor Field-Effect Transistors

J. P. Ashton[1,a)], P. M. Lenahan[1,b)], D. J. Lichtenwalner[2,c)], A. J. Lelis[3,d)], and M. A. Anders[4,e)]

[1]*The Pennsylvania State University, University Park, PA 16802, USA*

[2]*Wolfspeed, a Cree Company, 3028 E. Cornwallis Rd, Research Triangle Park, NC 27709, USA*

[3]*United States Army Research Laboratory, 2800 Powder Mill Road, Adelphi, MD 20783, USA*

[4]*National Institute of Standards and Technology, 100 Bureau Dr, Gaithersburg, MD 20899, USA*

a)   Corresponding author: jpa5108@psu.edu

We report on the effects of barium interfacial layer deposition and nitric oxide anneals on interface/near-interface defects in 4H-SiC metal-oxide-semiconductor field-effect transistors utilizing electrically detected magnetic resonance (EDMR). The 4H-SiC/SiO$_2$ interface has a large number of electrically active defects which reduce the effective channel mobility. Various passivation schemes have been utilized to decrease the interface defect density and thus increase the mobility. Two passivation schemes of great interest are post-oxidation annealing in nitric oxide (NO) and deposition of a barium interfacial layer (IL) before oxide growth. Our measurements compare the chemical nature of defects very near the 4H-SiC/SiO$_2$ interface in devices utilizing both passivation schemes and non-passivated devices. Both the NO anneal and the barium IL greatly reduce the interface region EDMR response, which corresponds to a large improvement in mobility. However, the EDMR response in devices subjected to the two passivation processes are somewhat different. We present results that suggest spin lattice relaxation times are longer in samples which received a barium IL than in samples with NO annealing; this result suggests a lower level of local strain within the vicinity of defects very near the 4H-SiC/SiO$_2$ interface in barium treated samples over NO annealed samples.

I. INTRODUCTION

4H-SiC/SiO$_2$ based metal-oxide-semiconductor field-effect transistors (MOSFETs) show great promise in high power and high temperature applications.[1,2] However, their promise is limited by the quality of the 4H-SiC/SiO$_2$ interface. Post-oxidation nitric oxide (NO) anneals substantially improve the interface, increasing the effective channel mobility by about an order of magnitude.[3] Quite recently, Lichtenwalner *et al.* showed that the addition of a barium (Ba) interfacial layer (IL), instead of an NO anneal, results in a doubling of mobility over NO anneals.[4,5] In order to understand the effects of Ba on trapping centers near the 4H-SiC/SiO$_2$ interface, as well as to develop a broader understanding of these passivating effects in general, we utilize electrically detected magnetic resonance (EDMR) measurements to study devices with both Ba and NO passivation

in comparison to devices which were not passivated with either Ba or NO anneals. (EDMR has been very successful in identifying defects in SiC devices.[3,6–10]) We utilize spin dependent recombination (SDR) via the bipolar amplification effect (BAE).[8,11] This technique probes near the middle of the SiC bandgap at and very near the SiC/SiO$_2$ interface.[8,11] BAE has been utilized in prior studies of the 4H-SiC/SiO$_2$ interface to elucidate information about the effect of NO anneals on defect density and mobility enhancement.[3,9] Although the BAE measurement detects levels in the vicinity of the middle of the SiC bandgap, a single variety of SiC defects can have multiple levels widely distributed in the gap. For example, several studies indicate that the SiC silicon vacancy, V$_{Si}$, has between four and six levels within the bandgap.[12–14] Thus, although our BAE measurements are specifically sensitive to defect levels in the vicinity of mid-gap, the detected defects can have levels widely distributed throughout the bandgap.[12–14]

The most obvious effect of both Ba and NO treatments is a very large reduction in the EDMR amplitude.[9] The dominating interface spectrum for the untreated devices is a silicon vacancy, V$_{Si}$.[6] Although the NO and Ba treatments have some effect on the (much smaller amplitude) spectra detected in those devices, silicon vacancies appear to be important in all cases. We also present SDR microwave power saturation measurements, which suggest that spin-lattice relaxation times (T$_1$) are longer in samples which received Ba treatment than in samples which received NO annealing. Longer T$_1$ times suggest that local strain is lower in the case of Ba treated samples than in the NO annealed samples.[15]

A. Electron Paramagnetic Resonance and Electrically Detected Magnetic Resonance

Electrically detected magnetic resonance is based on electron paramagnetic resonance (EPR). To understand the results presented, we provide a brief discussion of EPR. Consider a sample containing point defects with unpaired electron spins which is placed in a microwave cavity within an electromagnet. When a large magnetic field B is applied, the energy of electrons within these defects will be split into two levels. These levels are determined by the electron's spin quantum number, m_s, which can take on a value of +1/2 and -1/2. The sample is also subjected to a microwave field of magnitude B_1. In the simplest possible case, that is, when an unpaired electron is otherwise unaffected by its surroundings, when the microwave frequency ν times Planck's constant h is equal to that of the electron energy splitting (Zeeman splitting) $\Delta E = g_e \mu_B B$, the sample will absorb microwaves. Here, g_e is the Landè g factor ($g_e \approx 2.0023$), and μ_B is the Bohr magneton. At resonance, the electron transitions from its +1/2 to -1/2 spin state (or vice versa). For the simple case of an electron unperturbed by its local environment, the resonance condition is given by[16–18]:

$$hv = g_e \mu_B B. \qquad (1)$$

The analytical power of EPR (and EDMR) comes from deviations from this simplest of cases. For the spectra reported in this study, two phenomena dominate the deviations: (i) spin-orbit coupling and (ii) electron-nuclear hyperfine interactions, interactions between the electron and nearby nuclear magnetic moments. (This simple picture does not fully describe the defects under study here but does provide an introduction sufficient to understand the results of this paper.[6,19–21]) These interactions can be described via a spin Hamiltonian expressed as:

$$\mathcal{H} = \mu_B \boldsymbol{B} \cdot \boldsymbol{g} \cdot \boldsymbol{S} + \sum_i \boldsymbol{I}_i \cdot \boldsymbol{A}_i \cdot \boldsymbol{S}. \qquad (2)$$

Here, $\boldsymbol{B}$ is the applied magnetic field vector, $\boldsymbol{S}$ is the electronic spin operator, $\boldsymbol{I}_i$ is the nuclear spin operator for the ith nucleus, $\boldsymbol{g}$ is essentially a second rank tensor which is affected by the spin-orbit coupling interactions, and $\boldsymbol{A}_i$ is a tensor that describes the electron-nuclear hyperfine interactions. Analysis of resonance spectra in terms of (2) and other somewhat similar expressions allow definitive identification of the physical and chemical nature of defects. Although the mechanisms described by (2) are adequate to understand our results, other contributions to the resonance condition of (1) are possible and in fact are relevant to a full understanding of the defects under study here, but outside of the scope of this brief introduction.[6,19–21]

Conventional EPR has limitations in studies of micro- and nano-electronic systems. Conventional EPR has a sensitivity of about 10^{10} paramagnetic defects and is sensitive to all paramagnetic defects within the sample under study. Conventional EPR also has a sensitivity which is strongly dependent upon the field and frequency at which the measurements are made. Conventional EPR is also almost impossible at very low field and frequency. EDMR overcomes these limitations. In EDMR, we measure spin-dependent changes in device current at resonance. The sensitivity of EDMR can be about 1000 defects (possibly better) and only electrically active defects within the active area in the device under study are detected. Furthermore, the amplitude of the EDMR response amplitude is nearly frequency and field independent allowing multiple frequency EDMR measurements.

Multiple frequency EDMR measurements allow for a separation of the effects of spin-orbit coupling (on g) and hyperfine interactions.[8,22] For identical defects oriented identically in a magnetic field in a perfect crystalline environment, variations in the resonance condition due to g could not contribute to line broadening. However, in a crystalline environment that is somewhat disordered, a frequency dependent broadening involving variations in g is possible. One can understand the role of g by considering a defect with an axially symmetric g tensor: $g_{xx} = g_\parallel$; $g_{yy} = g_{zz} = g_\perp$. Assume that the range in g

determines the linewidth. If only a single defect orientation were to be present, only a single resonance field would appear. If the sample under study were polycrystalline or amorphous, all defect orientations would be present and the line broadening, ΔB, would be given by:

$$\Delta B \approx \frac{hv}{\mu_B} \left| \frac{g_\parallel - g_\perp}{g_\parallel g_\perp} \right|. \qquad (3)$$

Here, $g_\parallel$ and $g_\perp$ are the g tensor components of the defect aligned parallel and perpendicular to the applied magnetic field, respectively; h is Planck's constant, v is the microwave frequency, and μ_B is the Bohr magneton. We apply this logic to a system in which there is some variation in g, in this case due to some disorder in a crystalline environment. For the spectra under consideration here, the g tensor components are very close to 2; if we assume $g_\parallel \approx g_\perp \approx 2$, a range of g, Δg, can be estimated:

$$\Delta g \approx \frac{4\mu_B}{hv} \Delta B. \qquad (4)$$

Here, ΔB corresponds to the difference in the linewidth at high and very low magnetic field and frequency. The line broadening due to g observed at high field collapses at ultra-low magnetic fields. Thus, a measure of the relative disorder in a crystalline system can be obtained utilizing multiple frequency EDMR. In a perfect crystalline environment with only singly oriented defects, the g contribution to linewidth would be zero. However, if there is a range of g, Δg, due to disorder, (4) would provide a reasonable approximation to this value. We can thus obtain a measure of disorder from (4).

B. Spin Dependent Recombination

Trap-assisted recombination can be explained using the Shockley-Read-Hall (SRH) model.[23,24] Recombination takes place via defect energy levels around the middle of the semiconductor bandgap. An electron travelling through the conduction band is captured by a defect with a level near the middle of the bandgap. Subsequent hole capture results in electron-hole recombination. (Of course, this sequence may be reversed.) This process is spin dependent. A rudimentary explanation of the spin dependence is as follows.

If an electron encounters a deep level defect that is paramagnetic and both the conduction electron and unpaired electron have the same spin quantum number, capture of the conduction electron is not possible because the transition would violate the Pauli Exclusion Principle. However, at resonance, the trapped electron will "flip" spin, changing the spin quantum number from +1/2 to -1/2 (or vice versa). Now both trap level and conduction electrons have opposite spins and the conduction electron capture can occur. Thus, recombination at the site can occur, resulting in an increase in recombination current. SDR can be

more fully understood in terms of the seminal paper by Kaplan, Solomon and Mott (KSM)[25] and later refinements of this work.[26]

C. Bipolar Amplification Effect

The bipolar amplification effect (BAE) allows the SDR-based EDMR technique to be exclusively sensitive to defects very near the semiconductor dielectric interface which have energy levels near the middle of the bandgap.[11] In BAE, the source-body junction of the device is forward biased well past the built-in voltage and the gate bias is applied such that the semiconductor/oxide interface is in depletion, fairly close but not up to the inversion potential. The current through the drain is monitored with the drain held at virtual ground. The drain current is thus a combination of diffusion and recombination currents. The gate bias is applied such that some of the minority carriers are able to diffuse across the entire length of the channel. The BAE biasing scheme is illustrated in Fig. 1.
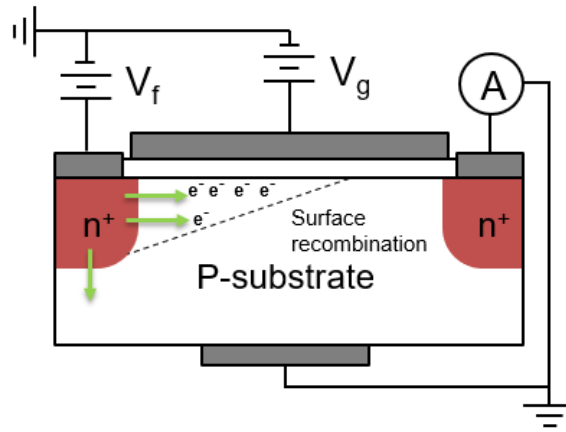
Fig. 1. Illustration of the BAE biasing scheme.

II. Experimental Details

Our measurements utilized SDR-BAE. Three different types of samples were utilized in these measurements. The untreated samples, which did not receive NO annealing or Ba IL, are planar structures with a 200 x 200 μm^2 gate area and have an effective channel mobility of about 6 cm^2/Vs. The NO annealed samples received a post-oxidation anneal in NO, are planar structures with a 200 x 200 μm^2 gate area, and were fabricated from n-type 4H-SiC with a p-type epitaxial channel region utilizing a thermal oxidation and a 1175 C NO anneal. The NO annealed samples' epitaxial regions were doped 5 x 10^{15} cm^{-3} p-type. The effective channel mobility for the NO annealed samples is about 20 cm^2/Vs.[4] The Ba treated samples are planar structures with a 200 x 200 μm^2 gate area, fabricated from n-type 4H-SiC with a p-type epitaxial channel region, and received a Ba IL via ultra-high vacuum molecular beam epitaxy at the SiC/SiO$_2$ interface before oxide growth.[4] The effective channel

5

mobility for Ba treated samples is about 40 cm^2/Vs.[4] Two EDMR spectrometer systems were utilized in our study. The first system utilized is a low-field/low-frequency EDMR spectrometer that consists of a Kepco BOP type bipolar power supply, a Lakeshore Cryogenics model 475 DSP Gauss meter and Hall probe, a custom-built electromagnet, a Agilent model 83732B synthesized signal generator for RF, a LabView based virtual lock-in amplifier and LabView based EDMR software. We use a computer equipped with a National Instruments data acquisition (DAQ) card. We utilize a Stanford Research Systems SR570 transimpedance preamplifier. The second system utilized is a high field EDMR spectrometer, which is based on a conventional X-band EPR spectrometer and consists of a Hewlett-Packard model 6268B DC power supply, a Micro-Now Instrument Co. model 8330A X-band microwave bridge, the same Gauss meter and Hall probe as utilized for low field EDMR, and the same preamplifier utilized for low field EDMR. The EDMR measurements were made at both high and low magnetic field and frequency. We utilize a proportional-integral controller to control the electromagnet via a power supply and Hall sensor.

III. Results and Discussion

Fig. 2 illustrates BAE measurements on all three types of samples at the same spectrometer gain and the same spectrometer settings. In all three cases, the device biasing conditions were chosen to maximize the EDMR response. Fig. 2 shows that with Ba treatment and NO annealing, there is a dramatic reduction in EDMR amplitude. The EDMR response from untreated samples is very large, whereas the responses from the Ba treated samples and the NO annealed samples is very small at this gain. The g value calculated for the NO annealed samples has an isotropic value of about 2.003, which is consistent with that of a silicon vacancy, V_{Si}.[6,19,20] The isotropic $g = 2.003 \pm 0.0003$ measured in our experiments is consistent with a dominating interface silicon vacancy, V_{Si}, defect. This isotropic g is not consistent with the anisotropic g tensor ($g_{\parallel} = 2.0023$ and $g_{\perp} = 2.0032$) corresponding to the 4H-SiC/SiO$_2$ carbon dangling bond.[27–29] The reduction in interface defect density should only very roughly scale with EDMR amplitude; however, it is reasonable to infer that the more than order-of-magnitude reduction in EDMR amplitude should correspond to a large reduction in defect density. (One should not expect a one-to-one correspondence between EDMR amplitude and defect density.) This result corroborates prior studies that have shown defect densities are lower in both NO annealed and Ba treated 4H-SiC MOSFETs.[5,8,30–32] The difference in EDMR amplitude from the untreated samples to the NO annealed samples and the Ba treated samples indicates that the NO anneals and Ba treatment both greatly reduce the number of interface defects, leading to an improvement in the quality of the 4H-SiC/SiO$_2$ interface. In Fig. 3, we increased the y-axis gain by a factor of 30 to observe the much smaller EDMR responses from only NO annealed and Ba treated samples. We note that in Fig. 3, the EDMR amplitude of the NO annealed samples is smaller than the EDMR amplitude of the Ba treated samples. However, at the bias utilized for this comparison, the DC current is larger in the Ba treated samples than in the NO annealed samples. To provide more information for the comparison of the effect of the Ba IL to the
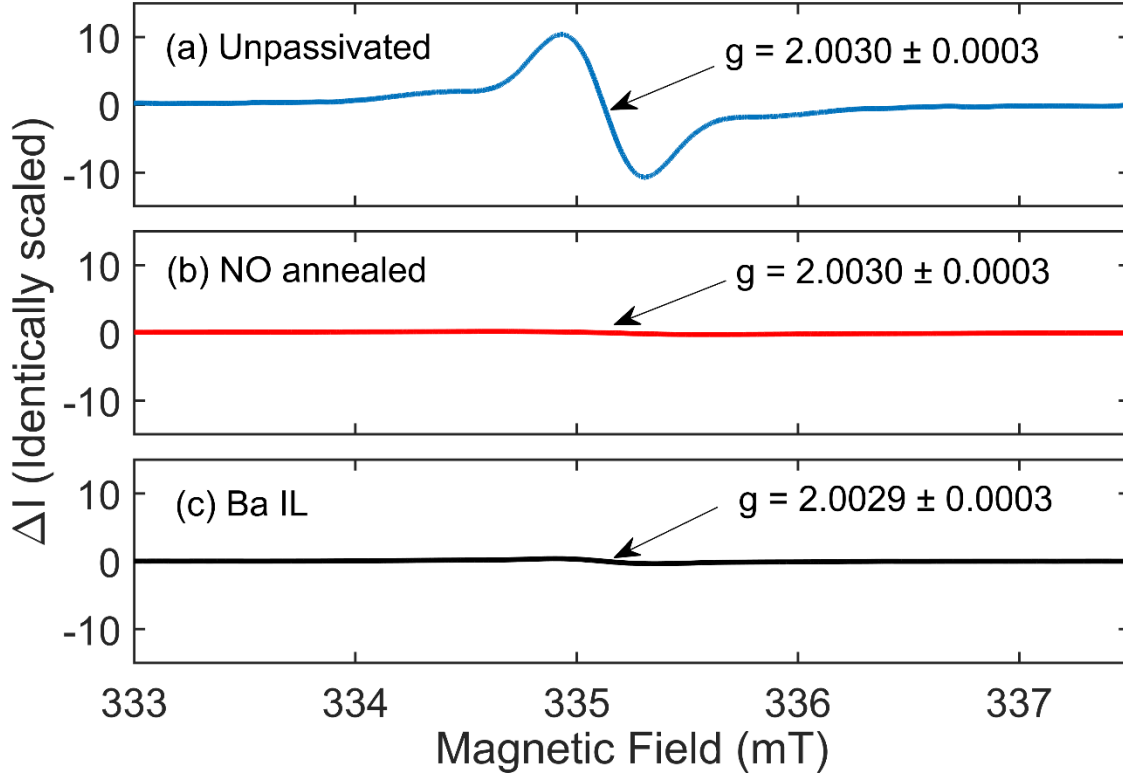
FIG. 2. X-band EDMR traces at the same gain for (a) untreated samples (6 cm^2/Vs), (b) NO annealed samples (20 cm^2/Vs), and (c) barium treated samples (40 cm^2/Vs). The center fields for the spectra were shifted to the center field of (a) the untreated samples. For (a), the x-band frequency was 9.395 GHz. For (b), the x-band frequency was 9.398 GHz. For (c), the x-band frequency was 9.402 GHz. The center-crossing g for all cases was 2.003 ± 0.0003.

effect of NO anneals on interface defect density, we compare the amplitude of the EDMR responses normalized by the DC current of the NO annealed samples to the Ba treated samples. A low field and frequency (151 MHz) EDMR BAE $\Delta I/I$ (SDR change in current over DC current) comparison of the NO annealed samples and Ba treated samples is presented in Fig. 4. Note that the $\Delta I/I$ for the Ba treated samples is less than for the NO annealed samples. This suggests but does not prove that the Ba treatment reduces the number of interface defects more than NO annealing. Furthermore, the BAE NO annealed spectrum reported here is also broader than spectra for NO annealed samples utilized in prior studies.[9] The NO annealed samples used here also show a significantly broader linewidth (0. 9 mT at X-band) than both the Ba treated sample spectrum and the untreated sample spectrum. The broadened line shape can be explained by considering that the local disorder is higher in these NO annealed samples and that hyperfine interactions with magnetic nitrogen nuclei also contributes to the observed broadening.[8]

Fig. 5, Fig. 6, and Fig. 7 show high field and frequency to low field and frequency comparisons for the untreated, NO annealed, and Ba treated samples respectively. Note that the traces of Fig. 5, Fig. 6, and Fig. 7 are all normalized to emphasize differences in line shape. We compare high and low field/frequency results using BAE. In each case, the plots are shifted from
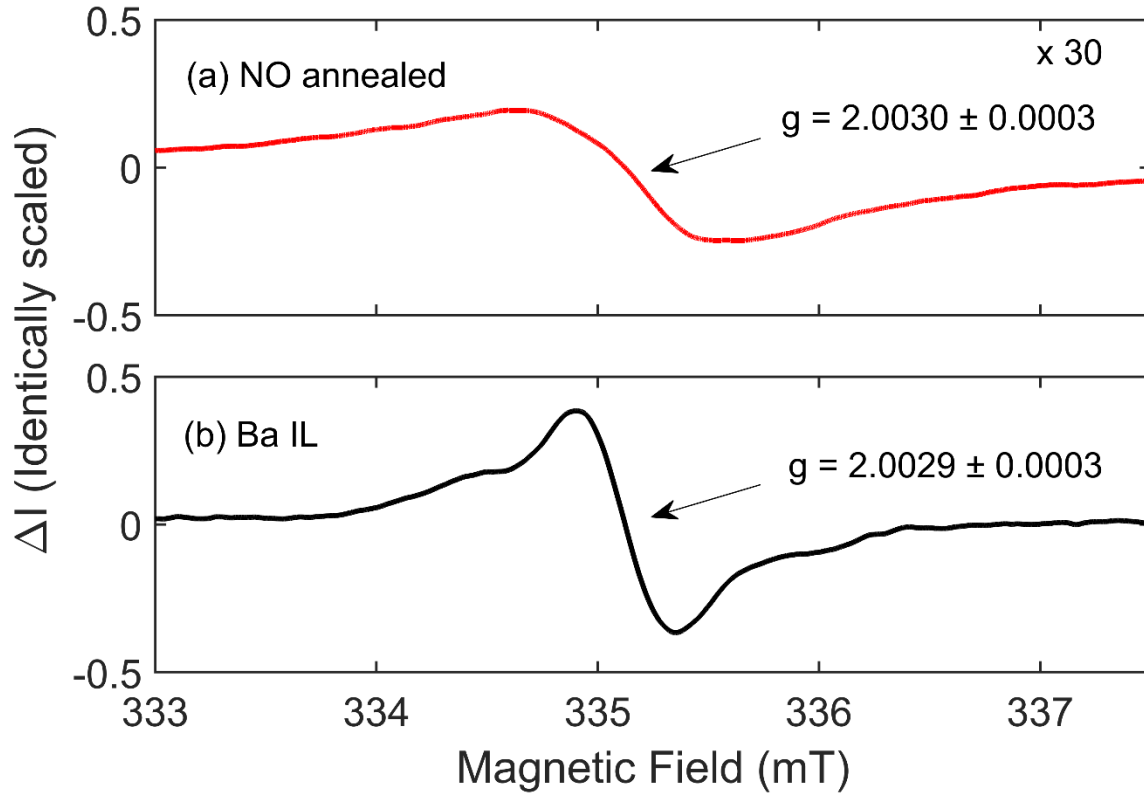
FIG. 3. X-band EDMR traces for the NO annealed samples (top – red), and barium treated samples (bottom – black) at an increase in gain of about 30 x. Again, the center fields for the spectra were shifted to the center field of the untreated samples from Fig. 2.
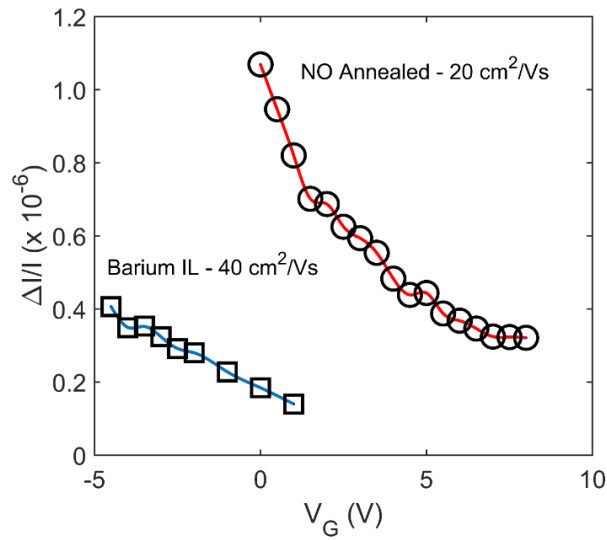
FIG. 4. $\frac{\Delta I}{I}$ vs. V_G for (blue curve-square markers) the barium treated samples and (red curve-circle markers) NO annealed samples. The interface defect EDMR response is more effectively reduced by Ba IL treatments than NO annealing.

the actual resonance field and centered at 0 mT to allow for comparison of the linewidths. Fig. 5 shows BAE high-field (9.4 GHz/335 mT) and ultra-low field (151 MHz/5.4 mT) spectra for the untreated samples. Fig. 6 shows BAE high-field (9.4
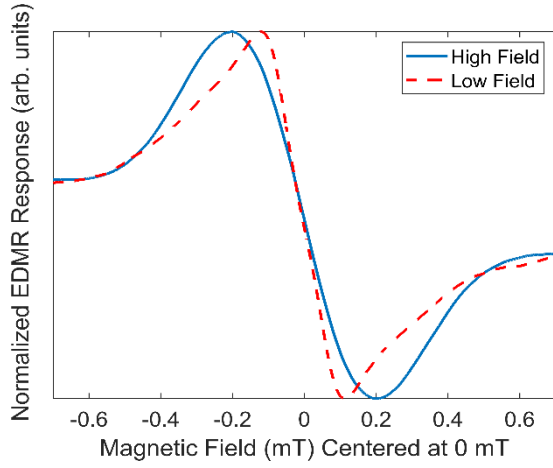
FIG. 5. (Dashed red line) Low field (151 MHz) and (solid blue line) high field (9.4 GHz) comparison for our BAE measurements for the untreated samples. The amplitudes have been normalized to emphasize line shape.
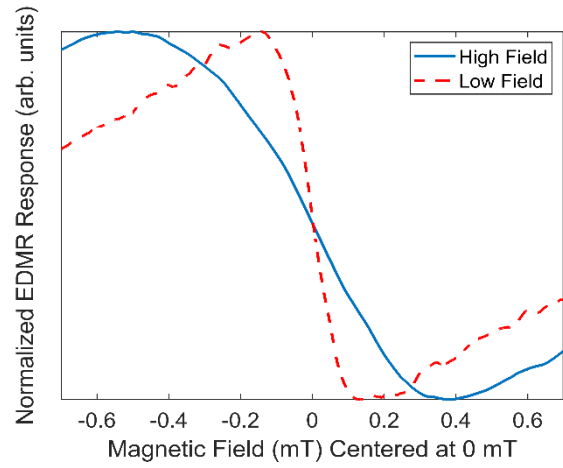
FIG. 6. (Dashed red line) Low field (151 MHz) and (solid blue line) high field (9.4 GHz) comparison for our BAE measurements for the NO annealed samples. The amplitudes have been normalized to emphasize line shape.
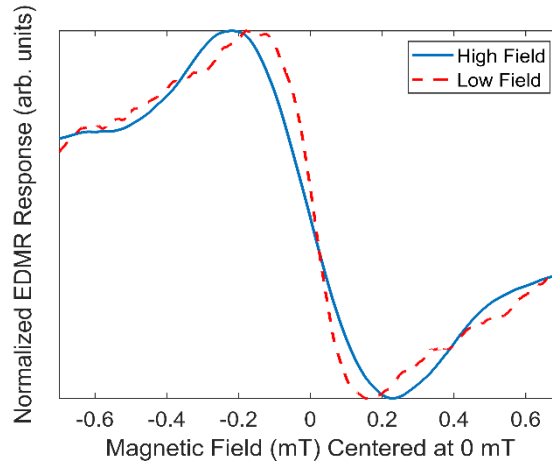
FIG. 7. (Dashed red line) Low field (151 MHz) and (solid blue line) high field (9.4 GHz) comparison for our BAE measurements for the Ba treated samples. The amplitudes have been normalized to emphasize line shape.

GHz/335 mT) and ultra-low field (151 MHz/5.4 mT) spectra for the NO annealed samples. Fig. 7 shows the BAE high field (9.4 GHz/335 mT) and ultra-low field (151 MHz/5.4 mT) spectra for the Ba treated samples. For the untreated samples, the high field linewidth is 0.4 mT and the low field linewidth is about 0.23 mT. The range in g for the untreated samples for BAE given by (4) is $\Delta g \approx 0.0010$. For the NO annealed samples, the high field linewidth is 0.9 mT and the low field linewidth is about 0.27 mT. The range in g for the NO annealed samples for BAE given by (4) is $\Delta g \approx 0.0038$. For the Ba treated samples, the high field linewidth is 0.45 mT and the low field linewidth is about 0.36 mT. The range in g for the Ba treated samples for BAE given by (4) is $\Delta g \approx 0.0005$. The high field linewidths, low field linewidths, and Δg values for all three sample types are given in table I. The center crossing g for all three samples is isotropic with a value of about 2.003, which is consistent with a silicon vacancy, V_{Si}.[6,19,20]

9

Table I. Summary of BAE high field/low field linewidths and approximate Δg for all three samples types

Samples	v_{HF}/v_{LF} (GHz)	High Field Linewidth (mT)	Low Field Linewidth (mT)	Δg
Untreated	9.4 / 0.151	0.4	0.23	0.0010
NO annealed	9.4 / 0.151	0.9	0.27	0.0038
Ba (IL) treated	9.4 / 0.151	0.45	0.36	0.0005

In untreated 4H-SiC MOSFETs, a strong centerline is observed centered about 335.2 mT that is almost certainly due to interface/near-interface silicon vacancies, $V_{Si,}$[6,8,33] with hyperfine side peaks separated by about 1.3 mT, equidistant from the centerline (these side peaks are observed at about 334.5 and 335.8 mT).[6] The side peaks are very likely due to hydrogen complexed E' centers; these E' centers are oxide defects involving silicon atoms that are back bonded to three oxygens often with a dangling bond facing into an oxygen vacancy.[34] E' centers have also been observed in more conventional Si/SiO_2 MOSFETs.[35] E' centers have been linked in the literature to the negative bias temperature instability.[36,37] With both NO annealing and Ba treatment, both the strong centerline spectrum (a V_{Si} spectrum), and the E' center spectrum are greatly reduced.

We also performed BAE EDMR measurements over a range of microwave power. The results are presented in Fig. 8. Here, we plot the normalized EDMR amplitude as a function of √microwave power (the curves were normalized by the EDMR amplitude at the highest power to emphasize the shapes of the curves). Microwave power saturation curves provide information regarding spin-lattice relaxation times T_1.[16] From Fig. 8, it is clear that the EDMR amplitude for the Ba treated samples saturates at a much lower power in comparison to the NO annealed samples. Since the Ba treated sample EDMR saturates at a much lower power in comparison with the NO annealed EDMR, it is likely that T_1 for Ba treated samples is longer than for NO
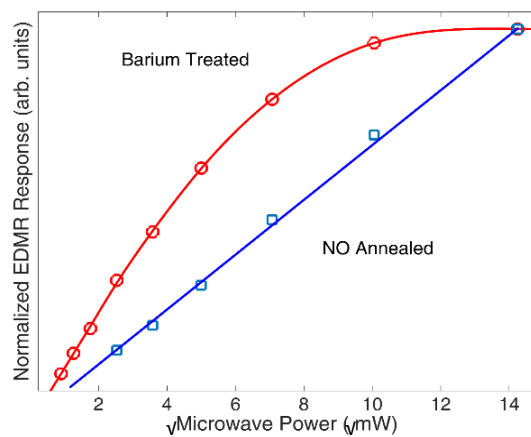
FIG. 8. Normalized √Microwave power vs. EDMR amplitude for barium treated (red curve – circle markers) and NO annealed (blue curve – square markers). Note that the EDMR amplitude saturates at much lower power for barium treated samples.

annealed samples.[38] An early paper by Castle *et al.*[15] showed that, for a SiO$_2$ oxygen vacancy defect (an E' center), T$_1$ could be related to local strain. A detailed interpretation of Fig. 8 is not straightforward because both the linewidth and spin-lattice relaxation times (T$_1$) of the defects under study will alter this response (EDMR amplitude saturation with microwave power depends on linewidth and T$_1$).[38] The more easily saturated EDMR response (that of the barium treated samples) is consistent with longer T$_1$, which is plausibly consistent with less local strain.[15] Less local strain would be consistent with the conclusions presented by Dycus *et al.*,[5] who argued that that local strain is absent with Ba treatment but is not with NO annealing. The lower level of local strain at the near-interface region in Ba treated samples implies that Ba treatment must not significantly distort the near-interface lattice, which suggests that Ba treatment more effectively passivates the 4H-SiC/SiO$_2$ interface.

The high field linewidth for the NO annealed sample EDMR spectrum, as shown in fig. 6, is much broader than the high field linewidth for the untreated and the Ba treated sample EDMR spectrum of fig. 5 and fig. 7 respectively (the high field linewidths for the untreated and Ba treated samples are the same within experimental error). This is caused by disorder at the 4H-SiC/SiO$_2$ interface, which leads to g broadening, and by unresolved hyperfine interactions due to high concentrations of nitrogen atoms introduced by NO to the interfacial region.[12]

IV. Conclusion

We have utilized EDMR via BAE to compare 4H-SiC MOSFETs which were untreated, received a Ba IL, and received NO anneals. We find that, with both Ba treatment and NO annealing, the amplitude of the EDMR response is dramatically reduced in comparison with untreated MOSFETs. Moreover, we compare the EDMR amplitudes normalized by the DC current of NO annealed samples and Ba treated samples and find that the Ba treatment reduces the EDMR response more than NO annealing. This result suggests, but does not prove, that the EDMR defect density is lower in the Ba treated samples than in the NO annealed samples. We compare high field and frequency EDMR and low field and frequency EDMR to look at g broadening and hyperfine interactions. The Δg results suggest the interface disorder is higher for NO annealed samples. Finally, we utilize microwave power saturation measurements to study the spin-lattice relaxation times, T$_1$, in both NO annealed and Ba treated MOSFETs. The results suggest that local near-interface strain is higher in NO annealed MOSFETs in comparison to MOSFETs with a Ba IL. It may be worth mentioning that the results presented herein are not consistent with dominating carbon dangling bond interface traps. This has been proposed in several recent publications.[27–29] One would expect that interface carbon dangling bonds would have an anisotropic g tensor with $g_{\parallel} \approx 2.0023$ and $g_{\perp} \approx 2.0032$. We measure an isotropic $g \approx 2.0030$; this isotropic g is consistent with what is observed for silicon vacancies.[6,19,33]

References

[1] J.B. Casady and R.W. Johnson, Solid. State. Electron. **39**, 1409 (1996).

[2] J. Biela, M. Schweizer, S. Waffler, and J.W. Kolar, IEEE Trans. Ind. Electron. **58**, 2872 (2011).

[3] M.A. Anders, P.M. Lenahan, C.J. Cochrane, and A.J. Lelis, IEEE Trans. Electron Devices **62**, 301 (2015).

[4] D.J. Lichtenwalner, L. Cheng, S. Dhar, A. Agarwal, and J.W. Palmour, Appl. Phys. Lett. **105**, 182107 (2014).

[5] J. Houston Dycus, W. Xu, D.J. Lichtenwalner, B. Hull, J.W. Palmour, and J.M. LeBeau, Appl. Phys. Lett. **108**, 201607 (2016).

[6] C.J. Cochrane, P.M. Lenahan, and A.J. Lelis, Appl. Phys. Lett. **100**, 023509 (2012).

[7] M.A. Anders, P.M. Lenahan, J. Follman, S.D. Arthur, J. McMahon, L. Yu, X. Zhu, and A.J. Lelis, in *IEEE Int. Integr. Reliab. Work. Final Rep.* (2014), pp. 16–19.

[8] M.A. Anders, P.M. Lenahan, and A.J. Lelis, J. Appl. Phys. **122**, 234503 (2017).

[9] C.J. Cochrane, P.M. Lenahan, and A.J. Lelis, Appl. Phys. Lett. **102**, 193507 (2013).

[10] T. Umeda, Y. Ishitsuka, J. Isoya, N.T. Son, E. Janzén, N. Morishita, T. Ohshima, H. Itoh, and A. Gali, Phys. Rev. B - Condens. Matter Mater. Phys. **71**, 193202 (2005).

[11] T. Aichinger and P.M. Lenahan, Appl. Phys. Lett. **101**, 083504 (2012).

[12] M.A. Anders, P.M. Lenahan, A.H. Edwards, P.A. Schultz, and R.M. Van Ginhoven, J. Appl. Phys. **124**, 184501 (2018).

[13] T. Hornos, Á. Gali, and B.G. Svensson, in *Mater. Sci. Forum* (2011), pp. 261–264.

[14] L. Torpo, M. Marlo, T.E.M. Staab, and R.M. Nieminen, J. Phys. Condens. Matter **13**, 6203 (2001).

[15] J.G. Castle, D.W. Feldman, and P.G. Klemens, Phys. Rev. B **130**, 577 (1963).

[16] W. Gordy, *Theory and Applications of Electron Spin Resonance* (John Wiley & Sons, 1980).

[17] C.P. Slichter, *Principles of Magnetic Resonance*, second (Springer, New York, 1978).

[18] J.A. Weil, J.R. Bolton, and J.E. Wertz, *Electron Paramagnetic Resonance - Elementary Theory and Practical Applications* (1994).

[19] T. Wimbauer, B. Meyer, A. Hofstaetter, and A. Scharmann, Phys. Rev. B - Condens. Matter Mater. Phys. **56**, 7384 (1997).

[20] C.J. Cochrane, P.M. Lenahan, and A.J. Lelis, in *Mater. Sci. Forum* (2012), pp. 433–436.

[21] P.G. Baranov, A.P. Bundakova, A.A. Soltamova, S.B. Orlinskii, I. V. Borovykh, R. Zondervan, R. Verberk, and J. Schmidt, Phys. Rev. B - Condens. Matter Mater. Phys. **83**, 125203 (2011).

[22] G. Joshi, R. Miller, L. Ogden, M. Kavand, S. Jamali, K. Ambal, S. Venkatesh, D. Schurig, H. Malissa, J.M. Lupton, and C. Boehme, Appl. Phys. Lett. **109**, 103303 (2016).

[23] W. Shockley and W.T. Read, Phys. Rev. **87**, 835 (1952).

[24] A.S. Grove, *Physics and Technology of Semiconductor Devices* (John Wiley & Sons, Berkeley, 1967).

[25] D. Kaplan, I. Solomon, and N.F. Mott, J. Phys. Lettres **39**, 51 (1978).

[26] F.C. Rong, W.R. Buchwald, E.H. Poindexter, W.L. Warren, and D.J. Keeble, Solid State Electron. **34**, 835 (1991).

[27] J.L. Cantin, H.J. von Bardeleben, Y. Shishkin, Y. Ke, R.P. Devaty, and W.J. Choyke, Phys. Rev. Lett. **92**, 015502 (2004).

[28] T. Umeda, G.W. Kim, T. Okuda, M. Sometani, T. Kimoto, and S. Harada, Appl. Phys. Lett. **113**, 061605 (2018).

[29] G. Gruber, J. Cottom, R. Meszaros, M. Koch, G. Pobegen, T. Aichinger, D. Peters, and P. Hadley, J. Appl. Phys. **123**, 161514 (2018).

[30] D.B. Habersat, A.J. Lelis, J.M. McGarrity, F.B. McLean, and S. Potbhare, in *Mater. Sci. Forum* (2009), pp. 743–746.

[31] G.Y. Chung, C.C. Tin, J.R. Williams, K. McDonald, M. Di Ventra, S.T. Pantelides, L.C. Feldman, and R.A. Weller, Appl. Phys. Lett. **76**, 1713 (2000).

[32] T. Umeda, K. Esaki, R. Kosugi, K. Fukuda, T. Ohshima, N. Morishita, and J. Isoya, Appl. Phys. Lett. **99**, 142105 (2011).

[33] N. Mizuochi, S. Yamasaki, H. Takizawa, N. Morishita, T. Ohshima, H. Itoh, and J. Isoya, Phys. Rev. B - Condens. Matter Mater. Phys. **66**, 235202 (2002).

[34] D.L. Griscom, Nucl. Instruments Methods Phys. Res. Bl 481 (1984).

[35] J.P. Campbell, S. Member, P.M. Lenahan, C.J. Cochrane, A.T. Krishnan, and S. Krishnan, IEEE Trans. Device Mater. Reliab. **7**, 540 (2007).

[36] P.M. Lenahan, M.A. Anders, R.J. Waskiewicz, and A.J. Lelis, Microelectron. Reliab. **81**, 1 (2018).

[37] A.J. Lelis, R. Green, and D.B. Habersat, in *Mater. Sci. Forum* (2011), pp. 599–602.

[38] G. Kawachi, C.F.O. Graeff, M.S. Brandt, and M. Stutzmann, Jpn. J. Appl. Phys. **36**, 121 (1997).